Title

Facile formation of van der Waals metal contact with III-nitride semiconductors

Journal

Science Bulletin, 69(23)

ISSN

2095-9273

Authors

Sun, Xiyu

Wang, Danhao

Wu, Xiaojing

et al.

Publication Date

2024-12-01

DOI

10.1016/j.scib.2024.09.028

Peer reviewed

Science Bulletin 69 (2024) 3692–3699

Contents lists available at ScienceDirect

Science Bulletin

journal homepage: www.elsevier.com/locate/scib

Article

Facile formation of van der Waals metal contact with III-nitride semiconductors

Xiyu Sun [a,1], Danhao Wang [a,1], Xiaojing Wu [b], Jiahao Zhang [a], Yangjian Lin [c], Dongyang Luo [a], Fang Li [a], Haochen Zhang [a], Wei Chen [a], Xin Liu [a], Yang Kang [a], Huabin Yu [a], Yuanmin Luo [a], Binghui Ge [b], Haiding Sun [a,*]

[a] iGaN Laboratory, School of Microelectronics, University of Science and Technology of China, Hefei 230029, China
[b] Information Materials and Intelligent Sensing Laboratory of Anhui Province, Institutes of Physical Science and Information Technology, Anhui University, Hefei 230601, China
[c] Instrumentation and Service Center for Physical Sciences, Westlake University, Hangzhou 310024, China

ARTICLE INFO

Article history:
Received 17 June 2024
Received in revised form 16 August 2024
Accepted 19 September 2024
Available online 24 September 2024

Keywords:
Van der Waals contact
GaN
Optoelectronics
Metal-semiconductor contact

ABSTRACT

Metal–semiconductor contacts play a pivotal role in controlling carrier transport in the fabrication of modern electronic devices. The exploration of van der Waals (vdW) metal contacts in semiconductor devices can potentially mitigate Fermi-level pinning at the metal–semiconductor interface, with particular success in two-dimensional layered semiconductors, triggering unprecedented electrical and optical characteristics. In this work, for the first time, we report the direct integration of vdW metal contacts with bulk wide bandgap gallium nitride (GaN) by employing a dry transfer technique. High-angle annular dark-field scanning transmission electron microscopy explicitly illustrates the existence of a vdW gap between the metal electrode and GaN. Strikingly, compared with devices fabricated with electron beam-evaporated metal contacts, the vdW contact device exhibits a responsivity two orders of magnitude higher with a significantly suppressed dark current in the nanoampere range. Furthermore, by leveraging the high responsivity and persistent photoconductivity obtained from vdW contact devices, we demonstrate imaging, wireless optical communication, and neuromorphic computing functionality. The integration of vdW contacts with bulk semiconductors offers a promising architecture to overcome device fabrication challenges, forming nearly ideal metal–semiconductor contacts for future integrated electronics and optoelectronics.

1. Introduction

Schottky metal–semiconductor contacts play crucial roles in the functionality and performance of modern semiconductor devices [1–3]. Nevertheless, Fermi-level pinning [4], arising from interface degradation associated with high-energy metal deposition [5–7], leads to a marked deviation of the observed Schottky barrier heights from the Schottky–Mott rule prediction [5,8,9]: for semiconductors with a defined work function, the difference in Schottky barrier heights across various types of metals is relatively small. Recently, nondestructive metallization methods, such as metal electrode lamination and inkjet printing techniques [10,11], have been demonstrated to enable the construction of damage-free metal–semiconductor interfaces, offering a novel approach to fully exploit the potential of Schottky contacts. Liu et al. [1] first developed a dry transfer approach to construct van der Waals (vdW) –contacted molybdenum disulfide (MoS_2) transistors, leading to highly tunable transistors approaching the Schottky–Mott limit. Thereafter, the proficient application of dry transfer techniques within two-dimensional material devices signifies the promising potential of this nondestructive approach for metallic integration [12–14]. For example, in photovoltaics, by creating high-performance vdW contacts on monocrystalline halide perovskite thin films, a three-order of magnitude reduction in contact resistance has been shown [15]. Nevertheless, although vdW contacts have been successfully applied in numerous material systems, their usage in commercially available bulk semiconductor platforms remains elusive.

In this work, for the first time, we integrate vdW metal contacts with wide-bandgap gallium nitride (GaN) via a simple dry transfer

* Correspondence author.
E-mail address: haiding@ustc.edu.cn (H. Sun).
[1] These authors contributed equally to this work.

https://doi.org/10.1016/j.scib.2024.09.028
2095-9273/

approach. The III-nitride materials have sparked considerable interest due to their tunable wide bandgap, high electron saturation velocity, excellent chemical stability, and scalability, rendering them indispensable materials in optoelectronics and power electronics [16–22]. Herein, we successfully transferred gold (Au) metal pads onto a GaN substrate. A 1-nm vdW gap can be clearly observed at the metal–semiconductor interface, as revealed by high-angle annular dark–field scanning transmission electron microscopy (HAADF-STEM), highlighting the damage-free nature of vdW metal contacts with an atomically flat morphology. Strikingly, the optoelectronic characteristics of vdW contact devices are significantly enhanced, achieving a two-order of magnitude increase in responsivity from 3.5 A/W to 979 A/W while increasing the photo-to-dark current ratio (PDCR) from 3.9 to 87 compared with a device with metal contacts fabricated via conventional electron beam (e-beam) evaporation. This improved performance of vdW contact devices is attributed primarily to the reduction in defects at the Au/GaN interface [7,23]. Furthermore, the high responsivity and persistent photoconductivity of the vdW contact device allow us to demonstrate its potential for imaging detection and optoelectronic neuromorphic applications. Our approach provides valuable insight into effectively controlling the contact situation as well as the interface quality between conventional bulk semiconductors and transferred metals, broadening the scope of optimization strategies for future integrated electronic and optoelectronic devices.

2. Materials and methods

2.1. Material growth

The epitaxial structure studied in this work was grown via metal–organic chemical vapor deposition (MOCVD) on the AMEC Prismo PD5® platform. The substrate was a 6-inch 1000-μm-thick silicon (Si) substrate with a resistivity (ρ) of 0.1 Ω·cm. The epitaxial growth started with high-temperature hydrogen (H_2) cleaning, and aluminum (Al) was predosed to prevent gallium (Ga) meltback. Then, a 200 nm aluminum nitride (AlN) nucleation layer was grown, followed by a 2.5-μm-thick composite aluminum gallium nitride (AlGaN) transition/buffer layer. The composite transition layer consisted of an AlN/AlGaN superlattice with an average Al composition of ∼70 %, an $Al_{0.35}GaN$ bulk layer, and an AlN/GaN superlattice with an average Al composition of ∼20 %. A 2-μm-thick GaN buffer was grown on top of the AlGaN transition layer. Both of the GaN and AlGaN buffer layers were doped with carbon at $\sim 1 \times 10^{19}$ cm^{-3} to form a high-resistance template. Then, 300-nm-thick Si-doped GaN (n-GaN) was grown at 1100 °C with a doping concentration of 10^{19} cm^{-3}. The sources for epitaxial growth included trimethylgallium (TMGa), trimethylaluminum (TMAl), ammonia (NH_3), and silicon tetrahydride (SiH_4).

2.2. Electrode transfer method

We first prepared metal electrodes via standard photolithography and e-beam evaporation on a sacrificial Si substrate. Next, we placed the wafer and metal electrodes in a hexamethyldisilazane (HMDS) atmosphere at 120 °C for 6 h to functionalize the whole wafer. Next, the poly(methyl methacrylate) (PMMA, A8 Mircochem Inc.) layer was spin-coated twice on top of the metal electrodes to form a 1-μm-thick PMMA layer on the sacrificial wafer. With prefunctionalization by HMDS, the PMMA layer has weak adhesion to the sacrificial substrate and can be mechanically released by using polydimethylsiloxane (PDMS Zhongke Experimental Materials), together with metal electrodes wrapped underneath. Then, the residual PMMA was removed by immersing the sample in acetone and isopropyl alcohol. Finally, the samples were rinsed with deionized water three times, and dried, yielding clean and undamaged electrode transfer devices.

2.3. Characterizations

HAADF-STEM and energy-dispersive spectroscopy (EDS) measurements were performed on a JEM-ARM200F instrument, and the samples were prepared through a focused ion beam (FIB). The optoelectronic responses of the device were examined on a semiconductor parameter system (4200SCS, Keithley). Light-emitting diodes (LEDs) (255, 265, 285, 310, 340, 365, 453, 520, and 625 nm) were used as the light sources, and the light intensities were calibrated by an optical power meter (S401C and PM100D).

3. Results and discussion

Fig. 1a illustrates the concept of this work. A high-quality wurtzite GaN thin film was grown via MOCVD on a 6-inch Si substrate. The room-temperature photoluminescence (PL) spectrum of the GaN film is shown in Fig. S1 (online). Fig. 1d depicts the dry transfer metallization process. Following standard photolithography, patterned Au electrodes were deposited on a sacrificial Si substrate (step i) [1]. Then, HMDS was applied to prefunctionalize the sacrificial Si substrate (Fig. S2 online), followed by spin-coating a PMMA layer. By rendering the Si surface hydrophobic through HMDS, the adhesive force between the PMMA and the sacrificial substrate can be effectively reduced, facilitating the complete detachment of metal electrodes via the use of PDMS (step ii). Subsequently, the released metal electrodes were subsequently physically laminated onto the GaN surface (step iii), followed by dipping into acetone and isopropyl alcohol to remove the PMMA layer (step iv). E-beam evaporated devices with identical electrode patterns were prepared for a comprehensive comparison, depicted in the upper half of Fig. 1a. Due to the high-energy deposition process in e-beam evaporation, the surface of GaN was damaged by the diffusion of Au atoms into GaN, as confirmed by HAADF-STEM imaging (Fig. 1b) and EDS mapping (Fig. S3 online). In contrast, the vdW contact shows a distinct 1 nm vdW gap between the Au electrode and the GaN surface, demonstrating an atomically sharp and damage-free metal–semiconductor interface (Fig. 1c). Previous research has indicated that defects at the metal–semiconductor interface are a leading cause of Fermi-level pinning, which in turn results in device performance degradation [7,24]. Conversely, the damage-free interface enables effective carrier transport, providing a perfect platform for constructing high-performance optoelectronic devices.

To elucidate the impact of interfacial defects on device performance, we constructed metal–semiconductor–metal (MSM) photodetectors by employing two different electrode fabrication approaches (Fig. 2a). Fig. 2b and c show the current–voltage (I–V) characteristic curves of the GaN photodetectors in the dark and under 340 nm ultraviolet illumination. Compared with the evaporated contact device, the vdW contact device substantially suppresses the dark current and significantly improves the photocurrent. We distilled the dark and light current values of both device types under variable biases, as illustrated in Fig. S4 (online). The marked discrepancy benefits from the presence of a vdW gap and the formation of a near-ideal Schottky junction, as the surface damage caused by the Fermi-level pinning effect at the Au/GaN interface has been significantly mitigated in vdW contact devices [25].

To further investigate the photoresponse behavior and explore the underlying mechanisms, time-dependent photoresponse

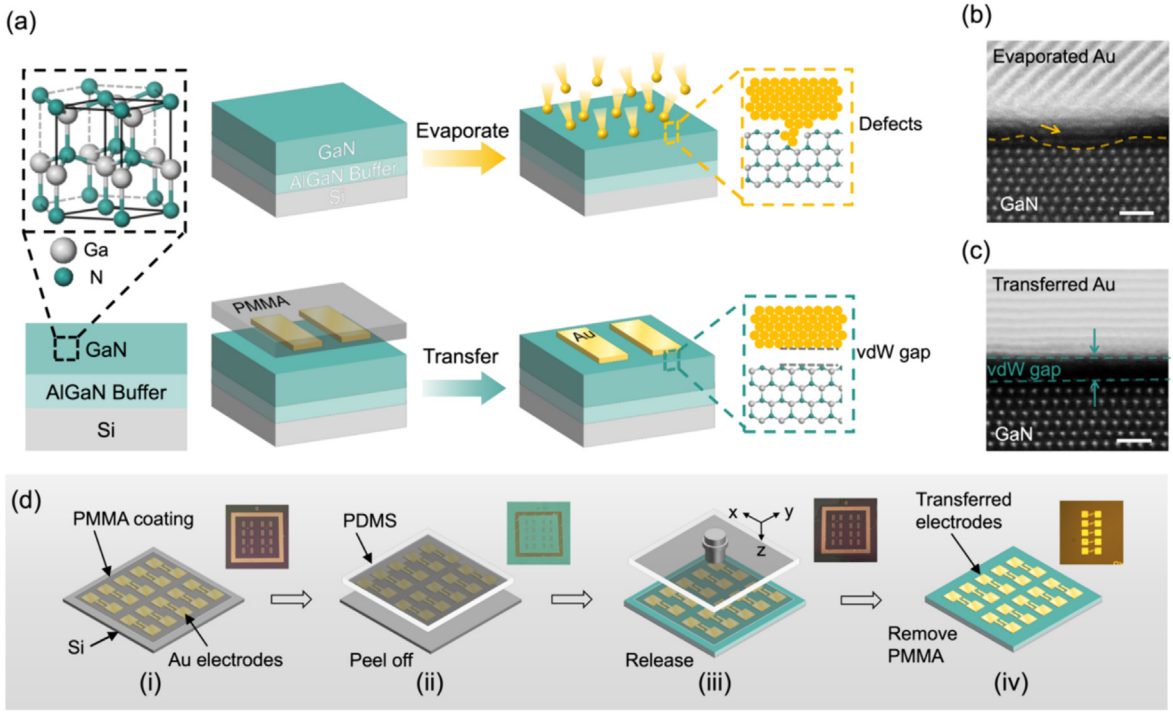

Fig. 1. (a) Schematic of metal contact deposition based on conventional e-beam evaporation and transfer of predeposited metal contacts. (b) Cross-sectional HAADF-STEM images of GaN with e-beam evaporation-fabricated and (c) dry transfer-fabricated Au electrodes. Scale bar, 1 nm. (d) Schematic illustration of the electrode dry transfer process. The insets show photographs and optical images of the transfer process of the Au matel electrodes. (i) Au electrodes deposited on a Si substrate. (ii) Au electrodes are physically released by a PDMS stamp with the assistance of PMMA. (iii) Au electrodes were transferred onto the target GaN substrate. (iv) After removing the PMMA, the Au electrodes were placed on GaN.

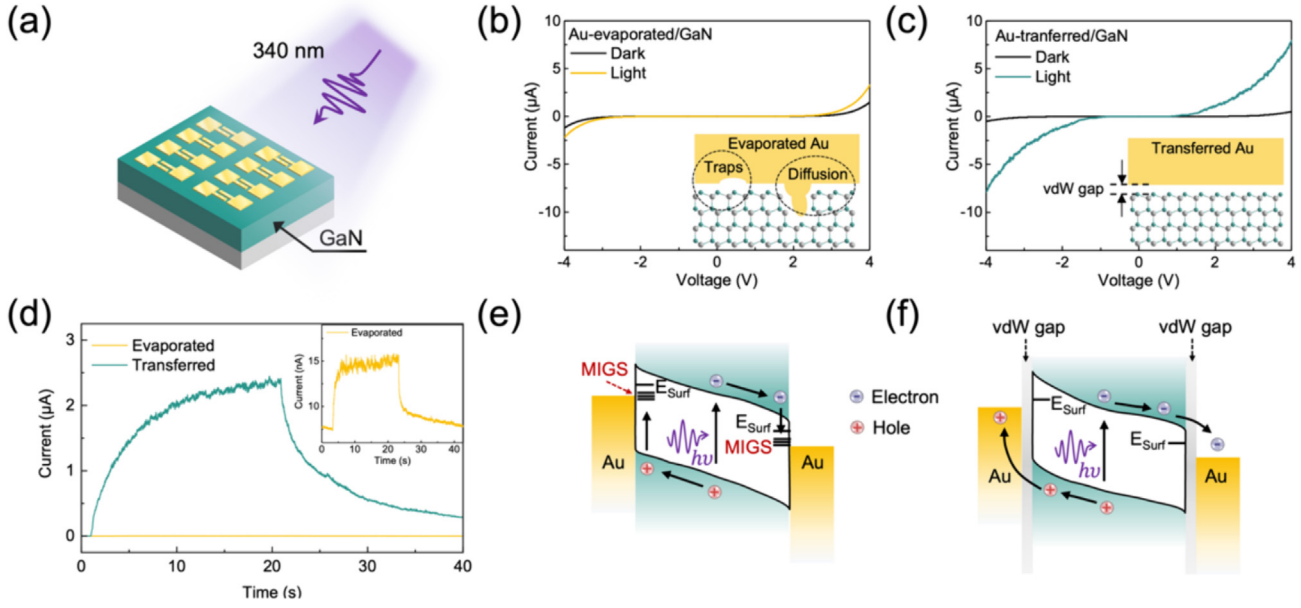

Fig. 2. (a) Schematic of the MSM photodetector under ultraviolet illumination (340 nm light emitting diode). I–V output characteristics in the dark and under 340 nm ultraviolet illumination with 0.26 mW/cm^2 light power intensity for (b) the evaporated contact device and (c) the vdW contact device. The inset figures show the schematics of Au/GaN interfaces of both the evaporated contact and the vdW contact device. (d) Time-dependent photoresponse of evaporated contact and vdW contact GaN photodetectors under 340 nm illumination with 0.26 mW/cm^2 light power intensity. The inset shows a magnified image of the time-dependent photoresponse of the evaporated contact GaN photodetector. (e) Energy band diagram for the evaporated contact device and (f) the vdW contact device under ultraviolet illumination. MIGS, E_{surf} and $h\nu$ represent metal-induced gap states, dangling bond-induced surface states and photons, respectively.

measurements were carried out, with one representative cycle presented in Fig. 2d. Under a fixed 2 V bias, the vdW contact device presents a remarkable photocurrent of 2.4 μA; in contrast, the photocurrent of the evaporated contact device is only 15 nA. Remarkably, the vdW contact device exhibits an enhanced responsivity of two orders of magnitude compared with that of the evaporated contact device, increasing from 3.5 A/W to 979 A/W. Notably, the vdW contact device exhibits longer response and

recovery times than the evaporated contact device does (Fig. S5, online), indicating persistent photoconductivity, which is promising for applications in optoelectronic synapses for neuromorphic image processing. The conventional metal deposition method, commonly afflicted by lithographic resist residues and high-energy deposition conditions, tends to induce interface defects caused by metal atom diffusion and material strain, fostering the emergence of metal-induced gap states (MIGSs) [1,7] (Fig. 2e). In contrast, the dry transfer technique enables the formation of a vdW gap between the semiconductor and transferred metal electrodes, weakening the Fermi-level pinning effect caused by the metal deposition process (Fig. 2f). In addition, even with a perfectly ordered surface atomic configuration, the existence of dangling bonds on the topmost atoms induces deviations in the surface energy states from the bulk electronic states, giving rise to surface states (E_{surf}) [26,27]. Due to the ultralow current levels near 0 V, fluctuations arising from the testing environment are challenging to eliminate, making accurate extraction of the barrier height from the voltage–current (I–V) characteristic curve difficult. To discuss the electronic performance of the vdW contact on GaN, we use a vertical Schottky diode as an example to obtain the barrier height of the evaporation contact and vdW contact devices [28,29] (more information can be found in Supporting Information Section II, online). At room temperature, the Schottky barrier height extracted from the vdW contact device is 0.97 eV, which is close to the theoretical value of 1 eV predicted by the Schottky–Mott rule (Au work function: 5.1 eV, GaN electron affinity: 4.1 eV) [30]. The slight deviation may be attributed to the unavoidable presence of dangling bonds on the GaN surface. In contrast, the Schottky barrier height for the device with evaporated contacts is approximately 0.89 eV, which is attributed to defect states at the Au/GaN interface. When illuminated by ultraviolet photons, photoexcited carriers are generated, and the bias drives the carriers directionally toward the electrodes. However, the metal evaporation-induced defects at the interface serve as recombination centers, diminishing the photocurrent and hastening carrier recombination [24,31–33]. Conversely, owing to its nondestructive interface properties, the vdW contact mitigates defect-related carrier recombination, leading to high responsivity and persistent photoconductivity. The persistent photoconductivity phenomenon in our vdW contact devices is a plausible way to explore optoelectronic neuromorphic functionality.

To further compare the photoelectronic properties of the evaporated contact and vdW contact devices, light intensity-dependent photoresponse measurements were carried out under both dark and illuminated conditions, as shown in Figs. 3a and b. A substantial increase in the photocurrent with increasing illumination intensity for both the evaporated contact and vdW contact devices was observed, indicating a clear power density-dependent photocurrent relationship. We further extracted the output photocurrent and calculated the responsivity (R) of the evaporated contact and vdW contact devices (Fig. 3c) via Eq. (1) [34–36]:

$$R = I_{ph}/(P \cdot S), \tag{1}$$

where photocurrent $I_{ph} = I_{light} - I_{dark}$ and where I_{light} and I_{dark} represent currents measured with and without illumination, respectively. P corresponds to the incident light power intensity (mW/cm^2), and S represents the effective area. Clearly, the vdW contact device exhibits a larger photocurrent and responsivity than the evaporated contact device, demonstrating a high responsivity of 979 A/W at 2 V, with a corresponding light power intensity of 0.18 mW/cm^2. To explore the device's uniformity and reproducibility, we provided the statistical distribution results of the responsivity for both the evaporation contact and the vdW contact samples in Fig. S6 (online).

Furthermore, several key figures of merit for comprehensively assessing device performance, such as PDCR and detectivity (D^*), were calculated and summarized [37,38]. The PDCR directly reflects the current ratio of the device under light and dark conditions and is calculated via Eq. (2):

$$\mathrm{PDCR} = (I_{light} - I_{dark})/I_{dark}. \tag{2}$$

Another important parameter, D^*, aimed at providing information regarding the signal-to-noise ratio, is obtained from Eq. (3):

$$D^* = RS^{1/2}/(2qI_{dark})^{1/2}, \tag{3}$$

where q is the absolute value of the electronic charge (1.6×10^{-19}C), under the assumption that the noise of the device is attributed mainly to the dark current. As illustrated in Fig. 3d the PDCR monotonically increases with increasing light power density because the number of photogenerated carriers increases with increasing light power intensity. D^* fluctuates slightly in the range of 4.76×10^{13} Jones to 5.58×10^{13} Jones and shows the highest detectivity of 5.58×10^{13} Jones under a 0.18 mW/cm^2 light power intensity. The wavelength-dependent photocurrent spectra were measured to further investigate the wavelength selectivity (Fig. 3e), where the vdW contact device demonstrated higher ultraviolet absorption. At a constant light intensity of 0.14 mW/cm^2, the wavelength-dependent PDCR of the photodetectors in the ultraviolet range is summarized in Fig. 3f, where the vdW contact device has a much higher PDCR for all illumination wavelengths. Furthermore, we extracted and calculated the device's optoelectronic performance under different applied biases, as shown in Fig. S7 (online). Both vdW contact and evaporated contact devices exhibit a wide photoresponse with the highest PDCR at approximately 340 nm and a falling edge at ~365 nm, corresponding to the intrinsic absorption of the GaN film (3.4 eV, corresponding to a wavelength of 364 nm), which is consistent with the results shown in Fig. 3e. Beyond a wavelength threshold of 400 nm, the detected photocurrent is negligible, indicating excellent visible-blind detection characteristics in GaN. Table S1 (online) lists the performances of representative wide bandgap semiconductor-based ultraviolet detectors reported in recent years. Our vdW contact device shows excellent responsivity and detectivity, suggesting the potential for significant advancements in ultraviolet photodetection and imaging applications.

To fully leverage the ultrahigh photoelectric detection capabilities of vdW contact devices, we conducted a series of experiments aimed at validating their application in visible-blind imaging. The imaging system is illustrated in Fig. 3g. We encoded the pattern information "GAN" in a 26×8 array and controlled the ultraviolet light source on–off states [39,40]. With the light on and off, the 1 and 0 signals are reflected in the device output current, followed by the data extraction process. Since the vdW contact device has the highest responsivity under 340 nm illumination, the output pattern shown in Fig. 3i is clearer, whereas the pattern is indiscernible under 453 nm illumination (Fig. 3h). This ultraviolet imaging demonstration manifests a remarkable photoresponse characteristic, underscoring the potential of vdW contact photodetectors for the development of optoelectronic devices for imaging systems.

By leveraging its high responsivity and inherent persistent photoconductivity, the vdW contact device can output continuously varying current states that depend on light and electrical parameters, enabling complicated neuromorphic functions, such as image contrast enhancement and Morse code transmission [41–44]. To simulate neurosynaptic functions, the dynamic optical response characteristics of the vdW contact device under various light power intensities were explored, as delineated in Fig. 4a. An increase in the memory level is noted with increasing learning

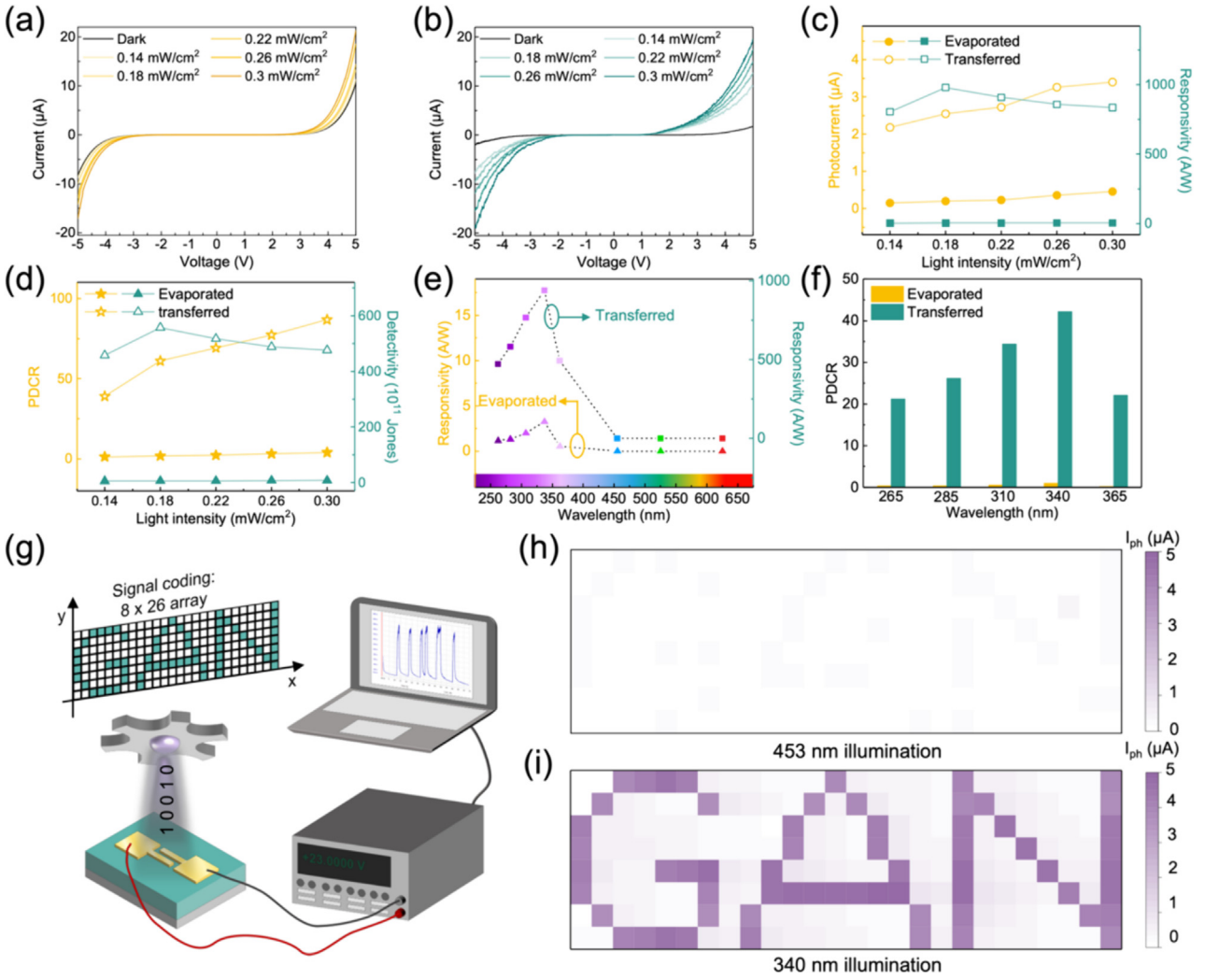

Fig. 3. I–V curves measured under various 340 nm illumination powers for (a) the evaporated contact device and (b) the vdW contact device. (c) Photocurrent and responsivity and (d) PDCR and D^* as a function of incident light power intensity for evaporated contact and vdW contact devices under 340 nm illumination. (e) Responsivity of evaporated contact and vdW contact GaN photodetectors under 265, 285, 310, 340, 365, 453, 520, and 625 nm light illumination with 0.26 mW/cm^2 light power intensity. (f) RDCR of the evaporated contact and vdW contact devices under different wavelengths of illumination. (g) Schematic diagram of an optical wireless imaging application with the input image displaying the characters "GAN". Results of the vdW contact device (h) under 453 nm and (i) 340 nm illumination.

intensity (light power intensity), indicating the retention characteristics of the vdW contact devices. This feature is harnessed to showcase image retention by projecting an "M" shape onto a 5 × 5 matrix. Images of the vdW contact device collected at different times after the removal of light stimulation are shown in Fig. 4b, where the output currents of the corresponding pixels are normalized (the weakest signals are normalized to 0 and the strongest signals are normalized to 1). The disparity in the output current intensifies over time, yielding a enhanced contrast in the image compared to the original input signal. Despite the presence of background noise, remarkable image retention is observed, suggesting excellent noise reduction and feature enhancement for various noise levels, underscoring the potential in artificial image processing.

Transmission of Morse code is also realized on the basis of the persistent photoconductivity phenomenon of vdW contact devices, exhibiting applicability in optical wireless communication. The Morse code transmission for all letters of the English alphabet (Fig. S8, online) and their specific combinations, such as "USTC GaN" (Fig. 4c), are achieved by encoding the optical signals with International Morse code [45]. Fig. 4d illustrates that the vdW contact device responds precisely to each letter of the English alphabet, demonstrating consistent excitatory postsynaptic current responses, which is indicative of potential in human–machine interface interactions. The adoption of vdW integration within GaN photodetector devices, enabling the exploration and realization of optoelectronic neuromorphic functionalities, such as image processing and wireless Morse code communication, represents a significant advancement in III-nitride-based optoelectronics and power electronics.

Finally, we would like to reemphasize that, prized for their bandgap tunability, high electron mobility, and compatibility with the semiconductor industry, III-nitride materials have been instrumental in the evolution of diverse functional devices across the fields of optoelectronics and power electronics [46]. Considering the intimate connection between the quality of metal–semiconductor contact interfaces and the performance of III-nitride–based devices, investigating the prospective application of vdW integration for metal electrodes in III-nitride material systems holds substantial practical importance [47]. For example, in III-nitride high-mobility field-effect transistors (HEMTs) [47–50], achieving an ideal Schottky contact between the gate and channel

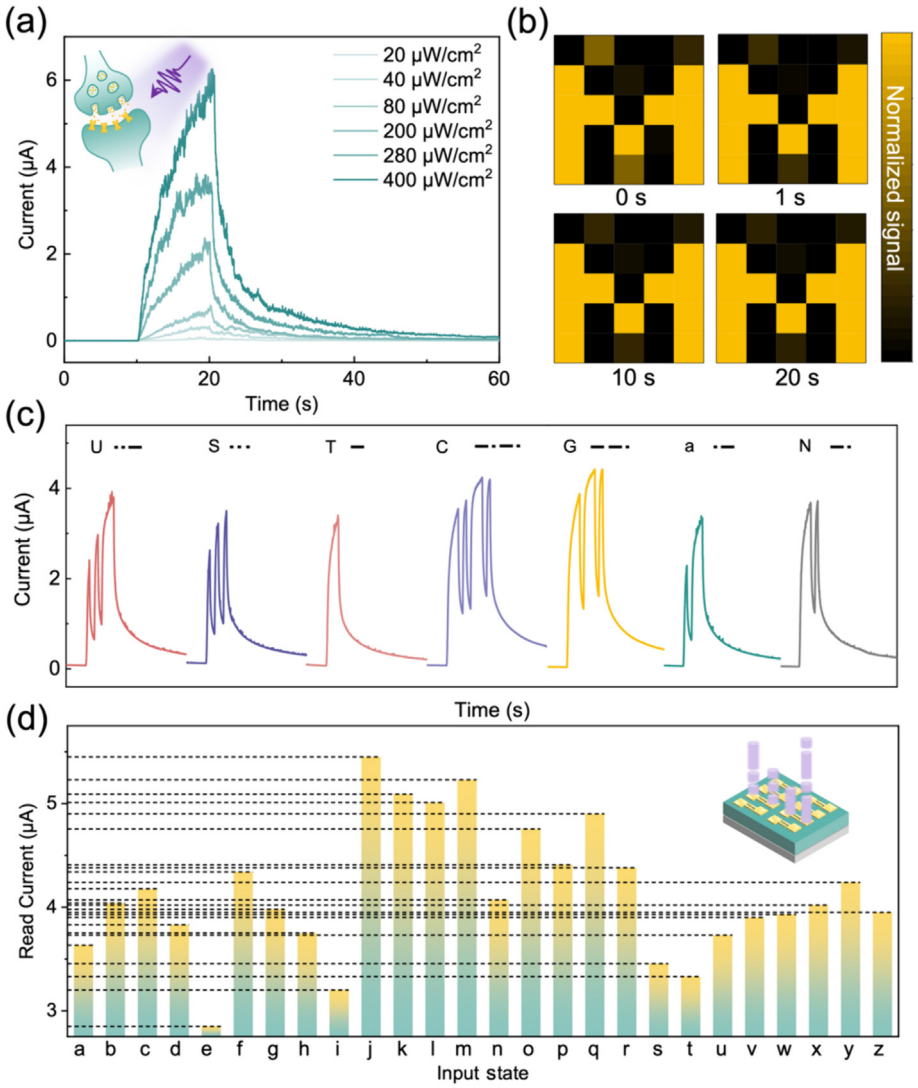

Fig. 4. Demonstrations of photosynaptic response applications. (a) Excitatory postsynaptic currents of a vdW contact device under different light power intensities. (b) Illustration of image contrast enhancement after training: memory of the 5 × 5 optoelectronic neuromorphic image "M" recorded after 0, 1, 10, and 20 s following light irradiation removal. (c) Excitatory postsynaptic current evoked by a series of spikes (340 nm, 0.26 mW/cm^2) representing the International Morse code of "USTC GaN" and (d) the International Morse code of every letter in the English alphabet. The spike durations of the dot and dash patterns are 1 s and 3 s, respectively, and the interval between two optical spikes is fixed at 1 s.

is imperative for averting leakage currents and preserving the gate control capability. Moreover, the quality of the metal–semiconductor interface in optoelectronic devices, such as LEDs, Schottky diodes, and photodetectors, profoundly affects the behavior of photogenerated carriers [51–53]. In addition, by employing advanced electron-beam lithography, the smallest size of vdW contacts can be achieved at approximately the tens of nanometers scale for possible high-density device integration with a reduced manufacturing cost [54]. The application of the dry transfer method to fabricate electrodes in the III-nitride material system will advance our comprehension of phenomena at material interfaces and further expand the application scenarios in the electronic and optoelectronic device fields, which holds considerable significance and novelty.

4. Conclusions

Herein, we report a vdW metal contact with wide bandgap GaN by forming a damage-free metal electrode via a dry transfer technique, which enabled the realization of superior optoelectronic characteristics, including neuromorphic functionality. HAADF-STEM clearly reveals a 1-nm-thick vdW gap at the metal–semiconductor interface, confirming the existence of an atomically flat, damage-free contact. The excellent photodetection performance of the vdW contact device (with a high responsivity of 979 A/W and a low dark current of 10^{-9} A) is attributed to defect reduction at the Au/GaN interface. Owing to the high responsivity and persistent photoconductivity of vdW contact devices, we further demonstrate their applications in image detection and optoelectronic neuromorphic functionality, including image contrast enhancement and Morse code communication. Our findings provide a facile and effective strategy to develop a high-quality interface between metal electrodes and semiconductors for future electronics and optoelectronics.

Conflict of interest

The authors declare that they have no conflicts of interest.

Acknowledgments

This work was funded by the National Natural Science Foundation of China (62322410, 52272168, and 52161145404) and was partially carried out at the USTC Center for Micro and Nanoscale Research and Fabrication.

Author contributions

Xiyu Sun and Danhao Wang contributed equally to this work. Haiding Sun conceived the idea and designed the experiments. Haochen Zhang performed MOCVD growth. Xiyu Sun, Jiahao Zhang, Fang Li, and Dongyang Luo fabricated the devices. Xiyu Sun and Jiahao Zhang carried out the photoresponse characteristic tests. Xiaojing Wu, Yangjian Lin, and Binghui Ge carried out the TEM characterizations. Xiyu Sun and Danhao Wang collected and analyzed the data. Xiyu Sun, Danhao Wang, and Haiding Sun wrote the initial draft of the manuscript, which was then revised by other coauthors. All of the authors have approved the final version of the manuscript.

Appendix A. Supplementary materials

Supplementary materials to this article can be found online at https://doi.org/10.1016/j.scib.2024.09.028.

References

[1] Liu Y, Guo J, Zhu E, et al. Approaching the Schottky-Mott limit in van der Waals metal–semiconductor junctions. Nature 2018;557:696–700.
[2] Werner JH, Güttler HH. Barrier inhomogeneities at Schottky contacts. J Appl Phys 1991;69:1522–33.
[3] Murali K, Dandu M, Watanabe K, et al. Accurate extraction of Schottky barrier height and universality of Fermi level de-pinning of van der Waals contacts. Adv Funct Mater 2021;31:2010513.
[4] Tung RT. Chemical bonding and Fermi level pinning at metal-semiconductor interfaces. Phys Rev Lett 2000;84:6078.
[5] Tung RT. The physics and chemistry of the Schottky barrier height. Appl Phys Rev 2014;1:011304.
[6] Bardeen J. Surface states and rectification at a metal semiconductor contact. Phys Rev 1947;71:717.
[7] Hasegawa H, Sawada T. On the electrical properties of compound semiconductor interfaces in metal/insulator/semiconductor structures and the possible origin of interface states. Thin Solid Films 1983;103:119–40.
[8] Schottky W. Zur Halbleitertheorie der Sperrschicht-und Spitzengleichrichter. Z Physik 1939;113:367–414.
[9] Mott NF. The theory of crystal rectifiers. Proc R Soc Lond A 1939;171:27–38.
[10] Loo YL, Someya T, Baldwin KW, et al. Soft, conformable electrical contacts for organic semiconductors: High-resolution plastic circuits by lamination. Proc Natl Acad Sci 2002;99:10252–6.
[11] Cho K, Lee T, Chung S. Inkjet printing of two-dimensional van der Waals materials: a new route towards emerging electronic device applications. Nanoscale Horiz 2022;7:1161–76.
[12] Wang Y, Chhowalla M. Making clean electrical contacts on 2D transition metal dichalcogenides. Nat Rev Phys 2022;4:101–12.
[13] Jang J, Ra HS, Ahn J, et al. Fermi-level pinning-free WSe_2 transistors via 2D van der Waals metal contacts and their circuits. Adv Mater 2022;34:2109899.
[14] Yang Z, Kim C, Lee KY, et al. A Fermi-level-pinning-free 1D electrical contact at the intrinsic 2D MoS_2–metal junction. Adv Mater 2019;31:1808231.
[15] Wang Y, Wan Z, Qian Q, et al. Probing photoelectrical transport in lead halide perovskites with van der Waals contacts. Nat Nanotechnol 2020;15:768–75.
[16] Wang D, Liu X, Kang Y, et al. Bidirectional photocurrent in p–n heterojunction nanowires. Nat Electron 2021;4:645–52.
[17] Fang S, Li L, Wang W, et al. Light-induced bipolar photoresponse with amplified photocurrents in an electrolyte-assisted bipolar p–n junction. Adv Mater 2023;35:2300911.
[18] Fang S, Wang D, Kang Y, et al. Balancing the photo-induced carrier transport behavior at two semiconductor interfaces for dual-polarity photodetection. Adv Funct Mater 2022;32:2202524.
[19] Wang D, Liu X, Fang S, et al. Pt/AlGaN nanoarchitecture: toward high responsivity, self-powered ultraviolet-sensitive photodetection. Nano Lett 2020;21:120–9.
[20] Luo Y, Wang D, Kang Y, et al. Demonstration of photoelectrochemical-type photodetectors using seawater as electrolyte for portable and wireless optical communication. Adv Opt Mater 2022;10:2102839.
[21] Wang D, Wu W, Fang S, et al. Observation of polarity-switchable photoconductivity in III-nitride/MoS_x core-shell nanowires. Light: Sci Appl 2022;11:227.
[22] Zhu S, Lin Z, Wang Z, et al. Vacuum-ultraviolet (λ< 200 nm) photodetector array. PhotoniX 2024;5:5.
[23] Liu Y, Stradins P, Wei SH. Van der Waals metal-semiconductor junction: Weak Fermi level pinning enables effective tuning of Schottky barrier. Sci Adv 2016;2:e1600069.
[24] Wu G, Chung HS, Bae TS, et al. Efficient suppression of charge recombination in self-powered photodetectors with band-aligned transferred van der Waals metal electrodes. ACS Appl Mater Interfaces 2021;13:61799–808.
[25] Luo PF, Liu C, Lin J, et al. Molybdenum disulfide transistors with enlarged van der Waals gaps at their dielectric interface via oxygen accumulation. Nat Electron 2022;5:849–58.
[26] Shockley W. On the surface states associated with a periodic potential. Phys Rev 1939;56:317.
[27] Segev D, Van de Walle CG. Origins of Fermi-level pinning on GaN and InN polar and nonpolar surfaces. Europhys Lett 2006;76:305.
[28] Dang K, Zhang J, Zhou H, et al. A 5.8-GHz high-power and high-efficiency rectifier circuit with lateral GaN Schottky diode for wireless power transfer. IEEE T Power Electr 2019;35:2247–52.
[29] Kim H. Vertical Schottky contacts to bulk GaN single crystals and current transport mechanisms: A review. J Electron Mater 2021;50:6688–707.
[30] Levinshtein ME, Rumyantsev SL, Shur MS, et al. Properties of advanced semiconductor materials: GaN, AlN, InN, BN, SiC, SiGe. John Wiley & Sons; 2001.
[31] Koba J, Koike J. Low contact resistivity of metal/n-GaN by the reduction of gap states with an epitaxially grown GaO_x insulating layer. AIP Adv 2022;12:085302.
[32] Zhao Q, Jie W, Wang T, et al. InSe Schottky diodes based on van der Waals contacts. Adv Funct Mater 2020;30:2001307.
[33] Kong L, Wu R, Chen Y, et al. Wafer-scale and universal van der Waals metal semiconductor contact. Nat Commun 2023;14:1014.
[34] Wang D, Huang C, Liu X, et al. Highly uniform, self-assembled AlGaN nanowires for self-powered solar-blind photodetector with fast-response speed and high responsivity. Adv Opt Mater 2021;9:2000893.
[35] Su W, Zhang S, Liu C, et al. Interlayer transition induced infrared response in ReS_2/2D perovskite van der Waals heterostructure photodector. Nano Lett 2022;22:10192–9.
[36] Long M, Wang P, Fang H, et al. Progress, challenges, and opportunities for 2D material based photodetectors. Adv Funct Mater 2019;29:1803807.
[37] Qin Y, Long S, Dong H, et al. Review of deep ultraviolet photodetector based on gallium oxide. Chin Phys B 2019;28:018501.
[38] Sun X, Wang D, Memon MH, et al. Anisotropic photoresponse behavior of a $LaAlO_3$ single-crystal-based vacuum-ultraviolet photodetector. Nanoscale 2022;14:16829–36.
[39] Jia L, Cheng L, Zheng W. 8-nm narrowband photodetection in diamonds. Opto-Electron Sci 2023;2:230010–1.
[40] Zhang H, Liang F, Yang L, et al. AlGaN/GaN-based photoimaging transistors and arrays with reconfigurable triple-mode functionalities enabled by voltage-programmed two-dimensional electron gas for high-quality imaging. Adv Mater 2024:2405874.
[41] Zhou F, Zhou Z, Chen J, et al. Optoelectronic resistive random access memory for neuromorphic vision sensors. Nat Nanotechnol 2019;14:776–82.
[42] Sun L, Qu S, Du Y, et al. Bio-inspired vision and neuromorphic image processing using printable metal oxide photonic synapses. ACS Photonics 2022;10:242–52.
[43] Yang B, Lu Y, Jiang D, et al. Bioinspired multifunctional organic transistors based on natural chlorophyll/organic semiconductors. Adv Mater 2020;32:2001227.
[44] Li G, Xie D, Zhong H, et al. Photo-induced non-volatile VO_2 phase transition for neuromorphic ultraviolet sensors. Nat Commun 2022;13:1729.
[45] Zhang J, Liu D, Shi Q, et al. Bioinspired organic optoelectronic synaptic transistors based on cellulose nanopaper and natural chlorophyll-a for neuromorphic systems. npj Flexible Electron 2022;6:30.
[46] Luo Y, Wang D, Kang Y, et al. Reprogrammable binary and ternary optoelectronic logic gates composed of nanostructured GaN photoelectrodes with bipolar photoresponse characteristics. Adv Opt Mater 2023;11:2300129.
[47] Sun Y, Zhang H, Yang L, et al. Correlation between electrical performance and gate width of GaN-based HEMTs. IEEE Electron Device Lett 2022;43:1199–202.
[48] Kajen RS, Bera LK, Tan HR, et al. Formation of Ni diffusion-induced surface traps in GaN/$Al_xGa_{1-x}N$/GaN heterostructures on silicon substrate during gate metal deposition. J Electron Mater 2016;45:493–8.
[49] Whiting PG, Holzworth MR, Lind AG, et al. Erosion defect formation in Ni-gate AlGaN/GaN high electron mobility transistors. Microelectron Reliab 2017;70:32–40.
[50] Du C, Ye R, Cai X, et al. A review on GaN HEMTs: nonlinear mechanisms and improvement methods. J Semicond 2023;44:121801.

[51] Yu H, Memon MH, Wang D, et al. AlGaN-based deep ultraviolet micro-LED emitting at 275 nm. Opt Lett 2021;46:3271–4.
[52] Wong MH. A landscape of β-Ga_2O_3 Schottky power diodes. J Semicond 2023;44:091605.
[53] Memon MH, Yu H, Luo Y, et al. A three-terminal light emitting and detecting diode. Nat Electron 2024:1–9.
[54] Yang X, Li J, Song R, et al. Highly reproducible van der Waals integration of two-dimensional electronics on the wafer scale. Nat Nanotechnol 2023;18:471–8.

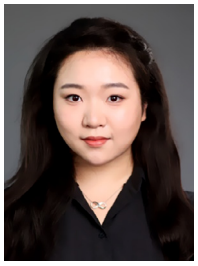

Xiyu Sun received her bachelor's degree from the Department of Materials Science and Engineering at Southern University of Science and Technology in 2022. After being a research assistant at University of Science and Technology of China, she is currently pursuing her Ph.D. degree at the Department of Electrical and Computer Engineering, University of California, San Diego. Her research focuses on novel semiconductor materials and device fabrication.

Danhao Wang received his Ph.D. degree from University of Science and Technology of China in 2022, followed by postdoctoral research at University of Michigan. His research primarily focuses on III-nitride material-based optoelectronic devices.

Haiding Sun received his Ph.D. degree in Electrical Engineering from Boston University. He is a Professor and PI for iGaN Laboratory at University of Science and Technology of China. His research interests include the investigation of the physics, MBE and MOCVD epitaxy, fabrication, and characterization of semiconductor materials and devices.